

# U-Net-based surrogate modeling for attosecond X-ray free-electron lasers

Yufei Wei<sup>1,2</sup> · Bingyang Yan<sup>1,2</sup> · Chenzhi Xu<sup>1,2,5</sup> · Jiawei Yan<sup>4†</sup> · Haixiao Deng<sup>3‡</sup>

the date of receipt and acceptance should be inserted later

**Abstract** Attosecond X-ray pulse generation in modern X-ray free-electron lasers relies on strongly compressed, precisely tailored electron bunches, making accurate diagnostics and control of the longitudinal phase space (LPS) essential. In the self-chirping scheme, collective effects in the linac generate a strong energy chirp that is converted into high peak current through pre-undulator compression, enabling isolated attosecond pulse generation. Reliable operation of this scheme depends on precise LPS control and fast diagnostics. In this work, we present a U-Net-based neural network surrogate that predicts two-dimensional LPS distributions directly from accelerator settings. The model exhibits excellent agreement with start-to-end simulation results. These results demonstrate the potential of neural network surrogates to facilitate real-time tuning and control in attosecond X-ray pulse generation.

## 1 Introduction

Relativistic electron beam driven light sources, including synchrotron radiation facilities and X-ray free-electron lasers (XFELs), are essential tools across physics, chemistry, materials science, and structural biology. Modern XFELs deliver ultrashort, high brightness X-ray pulses that enable time-resolved measurements on atomic length scales and femtosecond time scales [1]. A central frontier is to extend this control to the attosecond regime and to deliver user relevant pulse formats with reliable shot-to-shot stability. Achieving

that goal requires electron beam phase space control with increasingly demanding precision.

In recent years, a wide range of attosecond XFEL concepts has been proposed and demonstrated by shaping the electron beam longitudinal phase space (LPS) to create a narrow, high current region that dominates the FEL interaction. For example, the self-chirping mode at the European XFEL demonstrated terawatt-scale hard X-ray pulses [2]. Moreover, the AttoSHINE project has been proposed to generate high-power attosecond XFEL with continuous-wave XFELs, such as the Shanghai High Repetition Rate XFEL and Extreme Light Facility (SHINE) [3].

Realizing and stabilizing such LPS-sensitive XFEL modes requires iterative optimization of machine settings and frequent feedback on the resulting phase space. A conventional approach is to rely on computationally intensive start-to-end simulations to scan the relevant parameter space, whereas such simulations are often time-consuming and resource-demanding. Experimentally, the LPS can be measured using an X-band transverse deflecting cavity (TCAV) combined with a dipole magnet, which streaks and disperses the bunch onto a screen to produce single-shot phase-space images [4]. While highly informative, TCAV-based diagnostics are inherently invasive and therefore cannot be deployed continuously during user operation, especially at high repetition rates. These limitations motivate fast surrogate approaches for LPS diagnostics and phase-space design.

Machine learning has become a practical tool for building data-driven surrogates in accelerator physics, ranging from Gaussian process regression to deep neural networks [5–7]. By learning nonlinear mappings directly from archived or actively sampled data, surrogate models provide fast approximations of computationally expensive simulations or experimentally inaccessible diagnostics, and have been successfully used for high-dimensional control problem [8]. Multi-objective Bayesian optimization has been applied on

<sup>1</sup> Shanghai Institute of Applied Physics, Chinese Academy of Sciences, Shanghai 201800, China. <sup>2</sup> University of Chinese Academy of Sciences, Beijing 100049, China. <sup>3</sup> Shanghai Advanced Research Institute, Chinese Academy of Sciences, Shanghai 201210, China. <sup>4</sup> Deutsches Elektronen-Synchrotron DESY, 22603 Hamburg, Germany. <sup>5</sup> European XFEL, Schenefeld 22869, Germany.

† Corresponding author: [jiawei.yan@desy.de](mailto:jiawei.yan@desy.de)

‡ Corresponding author: [denghx@sari.ac.cn](mailto:denghx@sari.ac.cn)

operating machines to tune beams and map trade-offs between pulse energy, bandwidth, and beam quality [9–11]. Complementary approaches, including evolutionary many-objective optimization, have also been explored [12]. In particular, neural-network surrogates have demonstrated shot-to-shot prediction of electron-beam LPS with good agreement to deflector-based measurements [13, 14], and similar approaches have been applied to infer photon pulse properties from fast diagnostics [15].

In this work, we develop a U-Net based neural network surrogate that predicts two dimensional LPS distributions directly from accelerator settings in the AttoSHINE. The model is trained on start-to-end simulations and evaluated using both image based and physics motivated metrics. The resulting surrogate provides a fast forward model for parameter scans toward target phase space structures, and it is a step toward real time, LPS aware tuning workflows for high peak power attosecond XFEL operation.

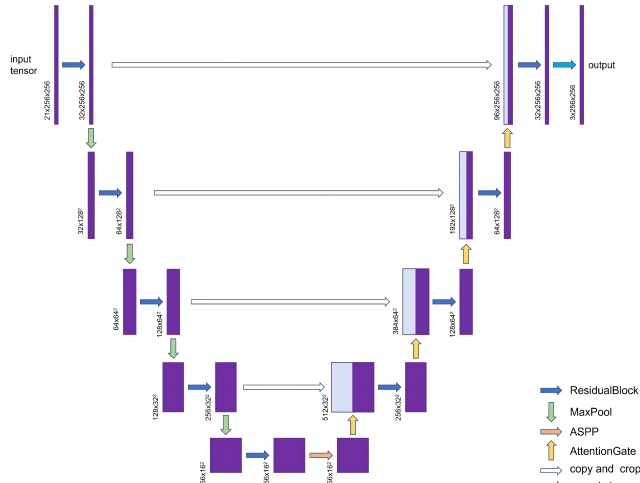


**Fig. 1** Schematic of the modified U-Net architecture. Feature maps are annotated as  $C \times H \times W$ . The encoder uses  $2 \times 2$  max pooling followed by residual blocks. The bottleneck includes an ASPP module. The decoder uses bilinear upsampling and attention gated skip fusion. Encoder features are concatenated with decoder features at matching scales, and padding is applied only when size alignment is required. A final  $1 \times 1$  convolution projects decoder features to the output density map.

## 2 Methods

U-Net is a fully convolutional encoder decoder architecture with skip connections, originally proposed by Ronneberger *et al.* for medical image segmentation [16]. By combining global context learned in the contracting path with high resolution features delivered through skip connections, U-Net is well suited for dense map prediction tasks that require both global structure and fine detail recovery. In this work,

we adopt a modified U-Net style backbone augmented with residual blocks [17], attention gated skip fusion [18], and multi-scale context aggregation via atrous spatial pyramid pooling (ASPP) [19].

The network architecture used in this study is shown in Fig. 1. The three accelerator phases form a length three conditioning vector, and each phase is broadcast to a constant two dimensional feature map so that the input can be processed by fully convolutional layers. We further concatenate explicit coordinate channels and sinusoidal positional encodings. Specifically, the normalized coordinates  $(x, y) \in [-1, 1]$  are appended as two additional channels, and Fourier style encodings are constructed using  $\sin(\pi f x)$ ,  $\cos(\pi f x)$ ,  $\sin(\pi f y)$ , and  $\cos(\pi f y)$  at frequencies  $f \in \{1, 2, 4, 8\}$  [20, 21]. The resulting tensor is fed into a symmetric encoder decoder with four downsampling stages and a bottleneck.

Each encoder stage applies a  $2 \times 2$  max pooling operation followed by a residual block comprising two  $3 \times 3$  convolutions, Group Normalization, and ReLU activations [22], together with an identity skip connection. When the number of channels changes, a  $1 \times 1$  projection is used on the residual branch to match dimensions [17]. At the bottleneck, an ASPP module composed of parallel atrous convolutions with multiple dilation rates expands the effective receptive field and captures multi scale context [19]. The decoder mirrors the encoder with four upsampling stages using bilinear upsampling, progressively restoring the resolution back to  $256 \times 256$ . At each decoder level, the corresponding encoder feature map is filtered by an attention gate before concatenation, enabling selective use of high resolution cues from the skip pathway [18]. If size alignment is required, padding is applied to the upsampled decoder features before concatenation. A final  $1 \times 1$  convolution produces the main prediction, matching the three channel representation used during training, where the same density map is replicated across channels for implementation convenience.

In addition to the main output, an auxiliary edge head attached to an intermediate decoder scale predicts a single channel edge proxy. The proxy target is computed from the reference density map using a Sobel type gradient operator, and the edge head is trained with an explicit edge supervision term. We also apply deep supervision using auxiliary prediction heads at multiple decoder scales, whose outputs are upsampled to the full resolution during training.

The overall training objective is a structure aware loss

$$L = L_{\text{rec}} + \lambda_g L_{\text{grad}} + \lambda_e L_{\text{edge}} + \lambda_{ds} L_{\text{ds}}, \quad (1)$$

where  $L_{\text{rec}}$  is a pixel wise reconstruction loss (L1) between prediction and target,  $L_{\text{grad}}$  enforces gradient consistency by comparing Sobel gradient magnitude maps of prediction and target,  $L_{\text{edge}}$  supervises the auxiliary edge head against the target gradient magnitude map, and  $L_{\text{ds}}$  is an average

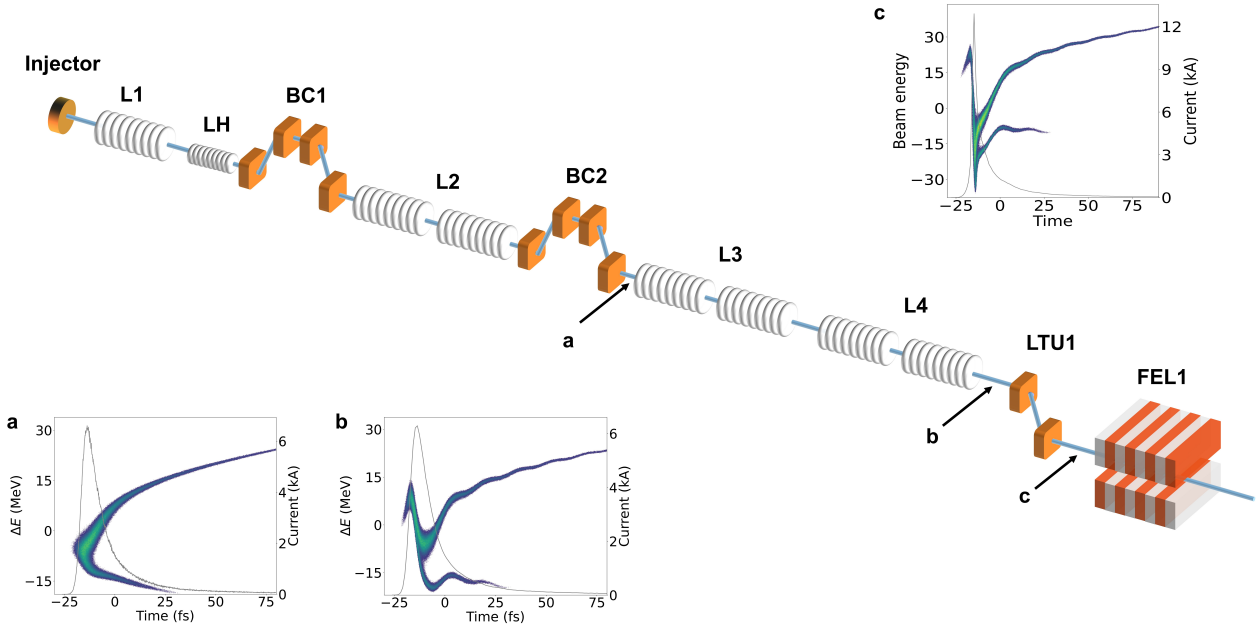


**Fig. 2** Schematic layout of the self-chirping process in AttoSHINE and the corresponding evolution of the electron-beam LPS. Insets show representative LPS distributions (colored density) together with the current profile (gray curve) at three locations along the beamline. (a) After nonlinear compression downstream of BC2. (b) At the end of L4. (c) After further compression in LTU1. The arrows labeled a–c indicate the corresponding observation points. The left is the head of the electron beam.

L1 loss over the multi scale auxiliary outputs. In our implementation we set  $(\lambda_g, \lambda_e, \lambda_{ds}) = (3.0, 1.0, 0.5)$ . The gradient based terms encourage the model to focus on structural discrepancies such as phase space boundaries rather than only matching intensity offsets.

### 3 Results of electron-beam prediction

To demonstrate LPS prediction capability, we consider the electron-beam manipulation in AttoSHINE. The layout and the corresponding LPS evolution during the self-chirping scheme are shown in Fig. 2. The layout consists of the linac sections L1, LH, L2, L3, and L4, the bunch-compression chicanes BC1 and BC2, the beam transport line LTU1, and the undulator section FEL1. As an illustrative example, we adopt a two-stage compression scheme. By tuning the RF phases in L1, LH, and L2, the bunch undergoes nonlinear compression after BC2, as shown in Fig. 2(a). By the end of the linac section L4, a pronounced energy chirp has developed along the bunch, as shown in Fig. 2(b). After further compression in LTU1, the bunch length is significantly shortened, as shown in Fig. 2(c), which is favorable for generating attosecond pulses. In this work, we take the LPS at location (b) as the prediction target and model the tuning of the RF phases in L1, LH, and L2. Throughout the simulations, the momentum compaction of the compression system is kept fixed. Starting from an optimized baseline case, we scan the three RF phases

within specified ranges. The scan ranges for each parameter are summarized in Table 1. This parameter scan yields a dataset of 10200 simulations performed with ELEGANT using  $10^5$  macroparticles per run. From the resulting samples, 8,000 are used for training, 2,000 for validation, and 200 are reserved as an independent test set. All results below are evaluated on the independent 200-case test set.

Parameters	Range
L1 phase	[-4.78, -4.38]
LH phase	[-141.81, -141.61]
L2 phase	[-33.64, -33.24]

**Table 1** Scan ranges of the three RF phase settings used as input features in the simulations. The phases of L1, LH, and L2 are varied while other lattice settings are kept fixed.

Figure 3 compares simulated and predicted current profiles obtained by projecting the LPS at the end of L4, onto the longitudinal axis. The neural-network predictions agree closely with the simulated profiles, as illustrated by the representative example in Fig. 3(a). Scatter comparisons of the peak current and the full width at half maximum (FWHM) between simulation and prediction show good agreement, as shown in Fig. 3(b) and (c). Across all tested cases, the mean relative differences between the predicted and simulated profiles are 0.95% for the peak current and 1.77% for the FWHM.

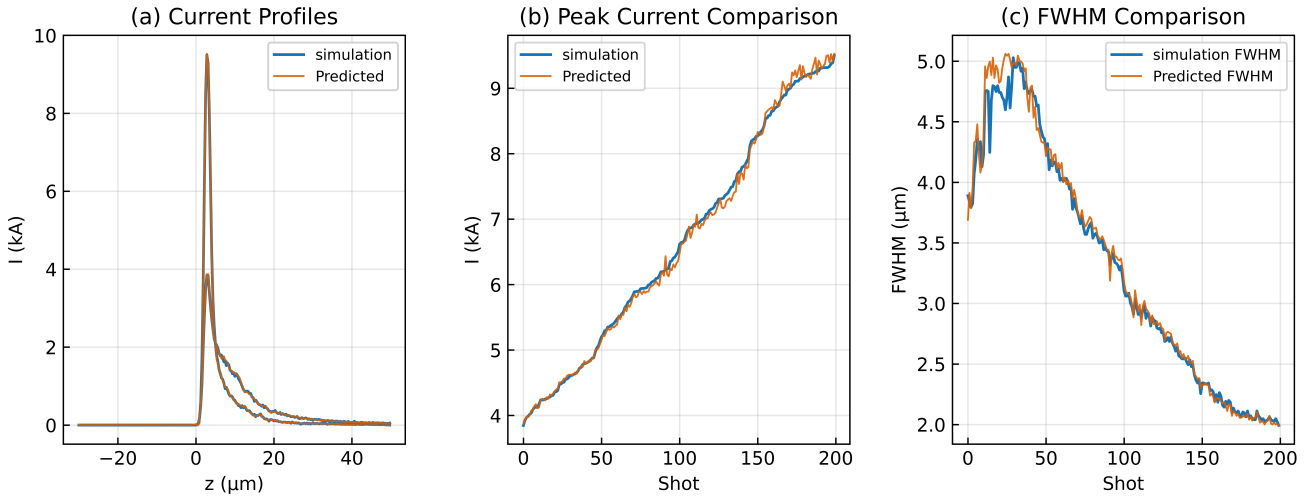


**Fig. 3** Comparison of simulated and U-Net-predicted current profiles derived from the LPS at the end of L4 (observation point (b) in Fig. 2) for the 200-case test set. (a) Representative reconstructed current profiles (including examples with the highest and lowest peak currents in the selected set). (b) Shot-by-shot comparison of peak current with shots sorted by the simulated peak current. (c) Shot-by-shot comparison of the full width at half maximum for the same shot ordering as in (b), showing the corresponding FWHM values for the peak-current-sorted cases. The close overlap between prediction and simulation indicates good agreement.

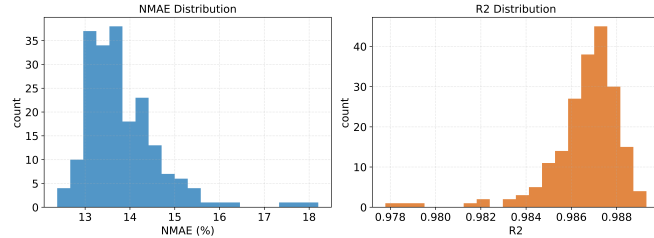


**Fig. 4** Histogram of the NMAE and  $R^2$  for 200 test set cases.

To provide a more physically intuitive and quantitatively rigorous validation, we evaluate the reconstruction accuracy using the normalized mean absolute error (NMAE) and the  $R^2$  score between the predicted images  $\hat{Y}$  and the ground-truth simulated images  $Y$ . They are defined as

$$\text{NMAE} = 100 \times \frac{\sum_{i,j} |Y_{ij} - \hat{Y}_{ij}|}{\sum_{i,j} |Y_{ij}|}, \quad R^2 = 1 - \frac{\sum_{i,j} (Y_{ij} - \hat{Y}_{ij})^2}{\sum_{i,j} (Y_{ij} - \bar{Y})^2}, \quad (2)$$

where  $i, j \in \{1, \dots, 256\}$  index pixel positions and  $\bar{Y}$  denotes the mean of  $Y_{ij}$  over all pixels for each simulated image. The resulting per-sample NMAE and  $R^2$  statistics for 200 test-set cases are summarized in Fig. 4. The mean ( $\pm$  rms) NMAE is  $13.83\% \pm 0.84\%$ , and the mean ( $\pm$  rms)  $R^2$  is  $0.9866 \pm 0.0016$ .

Figure 5 presents three representative test-set examples with NMAE values of 12.38%, 13.44%, and 18.21%, corresponding to the lowest-error case, a near-mean case, and the highest-error case, respectively. Reconstructions near

the mean error level ( $\sim 13\%$ ) reproduce the LPS structure with good visual fidelity. Even in the highest-error example (18.21%), the prediction preserves the dominant phase-space morphology, including the main high-current feature and fine-scale structures, and the resulting current profile remains qualitatively consistent with the start-to-end simulation, supporting its use for diagnostic interpretation.

In terms of computational efficiency, a single start-to-end ELEGANT simulation requires about 353 s on a laptop CPU (Intel(R) Core(TM) i7-10700, single core). By contrast, after training (performed on GPUs), a single surrogate evaluation takes approximately 150 ms on the same CPU core. Although the wall-clock time of start-to-end simulations can be reduced by parallel execution on multi-core clusters, high-fidelity studies often require macroparticle numbers in the  $10^6$  range (or higher) to suppress statistical noise, especially when resolving fine structures and low-density regions. This requirement increases the per-run simulation cost and further widens the computational advantage of the surrogate model for parameter scans and iterative tuning workflows.

## 4 Conclusions

We presented a U-Net-based surrogate that predicts two-dimensional electron-beam LPS distributions from a small set of accelerator phase settings for the AttoSHINE. The surrogate shows good agreement with start-to-end simulations in both the reconstructed current profiles and the full two-dimensional phase-space images, capturing the key LPS morphology relevant to attosecond operation. With low inference latency and high predictive accuracy, the model enables

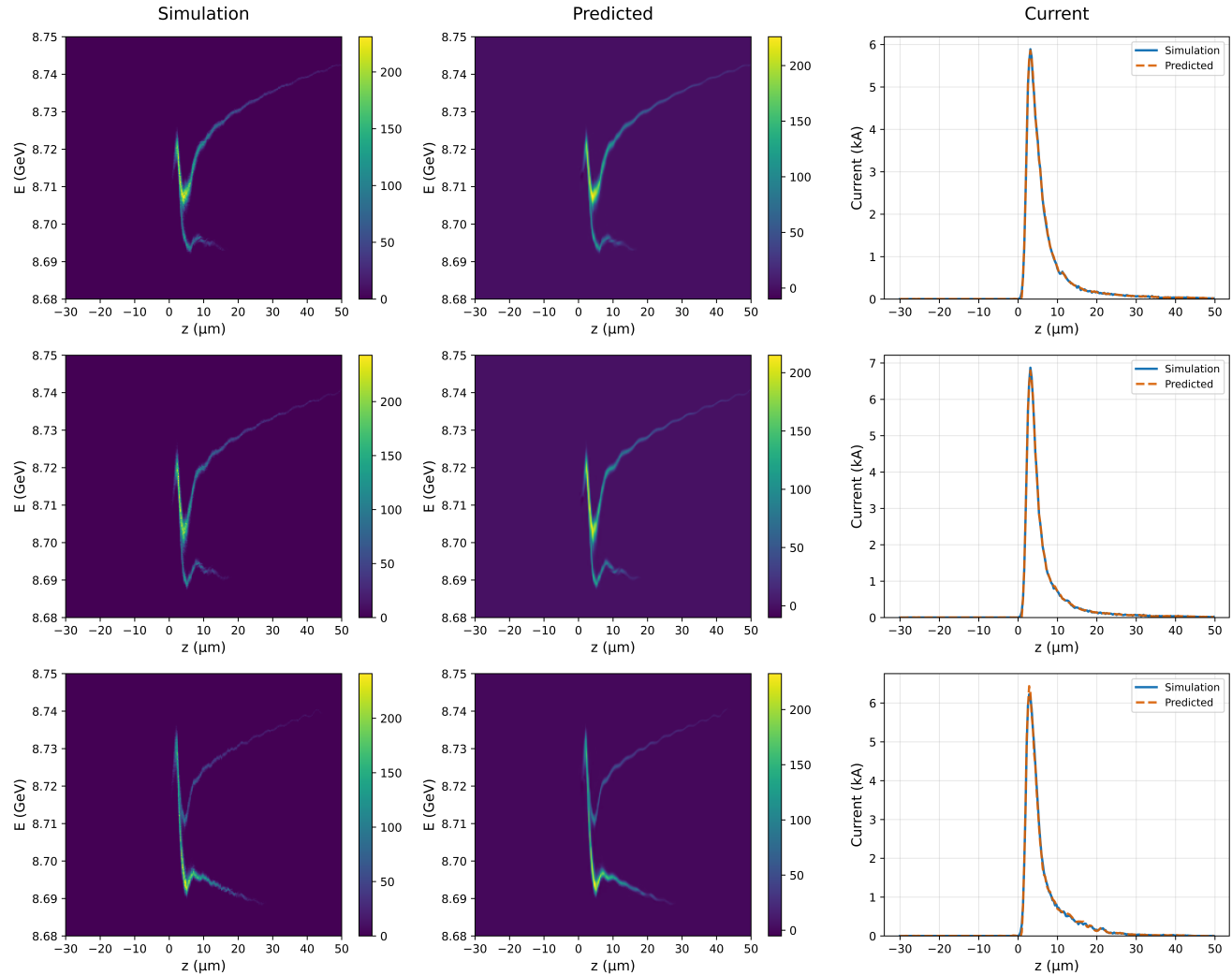


**Fig. 5** Three representative test-set examples. For each case, the left panel shows the simulated longitudinal phase space, the middle panel shows the U-Net prediction, and the right panel compares the corresponding current profiles from simulation and prediction. From top to bottom, the NMAE values in phase space are 12.38%, 13.44%, and 18.21%, respectively.

fast, non-invasive access to diagnostically relevant phase-space features and can serve as a practical forward model for real-time virtual diagnostics and data-efficient tuning workflows in routine accelerator operation.

Future work will focus on experimental validation and sim-to-real transfer, uncertainty quantification for reliability under drifts and out-of-distribution settings, and improved generalization across broader operating regimes and machine configurations. These developments will help establish AI surrogates as an enabling layer for robust commissioning and stabilization of LPS-sensitive attosecond XFEL modes at high repetition rates.

## 5 Acknowledgements

This work was supported by the National Natural Science Foundation of China (12125508, 12541503), the National

Key Research and Development Program of China (2024YFA1612104) and Shanghai Pilot Program for Basic Research – Chinese Academy of Sciences, Shanghai Branch (JCYJ-SHFY-2021-010). Jiawei Yan acknowledges support from DESY (Hamburg, Germany), a member of the Helmholtz Association (HGF), and the European XFEL (Schenefeld, Germany).

## 6 Data Availability Statement

Data supporting the findings of this study are available from the corresponding author upon reasonable request.

## References

1. Nanshun Huang, Haixiao Deng, Bo Liu, Dong Wang, and Zhentang Zhao. Features and futures of x-ray free-

electron lasers. *The Innovation*, 2(2):100097, 2021.

2. Jiawei Yan, Weilun Qin, Ye Chen, Winfried Decking, Philipp Dijkstal, Marc Guetg, Ichiro Inoue, Naresh Ku-jala, Shan Liu, Tianyun Long, Najmeh Mirian, and Gianluca Geloni. Terawatt-attosecond hard X-ray free-electron laser at high repetition rate. *Nature Photonics*, 18(12):1293–1298, 2024.
3. Bingyang Yan, Chenzhi Xu, Si Chen, Duan Gu, Ye Chen, Jiawei Yan, and Haixiao Deng. Attoshine: Generation of continuous-wave terawatt-scale attosecond x-ray pulses at shine, 2025.
4. J.W. Yan, H.X. Deng, B. Liu, and D. Wang. Transverse Deflecting Structure Dynamics for Time-Resolved Machine Studies of Shine. In *Proc. FEL'19*, number 39 in Free Electron Laser Conference, pages 632–634. JACoW Publishing, Geneva, Switzerland, nov 2019. <https://doi.org/10.18429/JACoW-FEL2019-THP018>.
5. Carl Edward Rasmussen and Christopher K. I. Williams. *Gaussian Processes for Machine Learning*. The MIT Press, 11 2005.
6. Yann LeCun, Yoshua Bengio, and Geoffrey Hinton. Deep learning. *Nature*, 521(7553):436–444, 2015.
7. Auralee Edelen, Nicole Neveu, Matthias Frey, Yannick Huber, Christopher Mayes, and Andreas Adelmann. Machine learning for orders of magnitude speedup in multiobjective optimization of particle accelerator systems. *Phys. Rev. Accel. Beams*, 23:044601, Apr 2020.
8. Ryan Roussel, Auralee L. Edelen, Tobias Boltz, Dylan Kennedy, Zhe Zhang, Fuhao Ji, Xiaobiao Huang, Daniel Ratner, Andrea Santamaria Garcia, Chenran Xu, Jan Kaiser, Angel Ferran Pousa, Annika Eichler, Jannis O. Lübsen, Natalie M. Isenberg, Yuan Gao, Nikita Kuklev, Jose Martinez, Brahim Mustapha, Verena Kain, Christopher Mayes, Weijian Lin, Simone Maria Liuzzo, Jason St. John, Matthew J. V. Streeter, Remi Lehe, and Willie Neiswanger. Bayesian optimization algorithms for accelerator physics. *Phys. Rev. Accel. Beams*, 27:084801, Aug 2024.
9. Ryan Roussel, Adi Hanuka, and Auralee Edelen. Multiobjective bayesian optimization for online accelerator tuning. *Phys. Rev. Accel. Beams*, 24:062801, Jun 2021.
10. Fuhao Ji, Auralee Edelen, Ryan Roussel, Xiaozhe Shen, Sara Miskovich, Stephen Weathersby, Duan Luo, Mianzhen Mo, Patrick Kramer, Christopher Mayes, Mohamed A. K. Othman, Emilio Nanni, Xijie Wang, Alexander Reid, Michael Minitti, and Robert Joel England. Multi-objective Bayesian active learning for MeV-ultrafast electron diffraction. *Nature Communications*, 15:4726, 2024.
11. Chenzhi Xu, Bingyang Yan, Gianluca Geloni, Jiawei Yan, Tianyu Long, and Haixiao Deng. High dimensional FEL performance optimization with infinite-width bayesian neural networks. In *Proceedings of the 16th International Particle Accelerator Conference (IPAC'25)*, pages 146–149, Taipei, Taiwan, 2025. JACoW Publishing.
12. Jiawei Yan and Haixiao Deng. Generation of large-bandwidth x-ray free electron laser with evolutionary many-objective optimization algorithm. *Phys. Rev. Accel. Beams*, 22:020703, Feb 2019.
13. C. Emma, A. Edelen, M. J. Hogan, B. O'Shea, G. White, and V. Yakimenko. Machine learning-based longitudinal phase space prediction of particle accelerators. *Physical Review Accelerators and Beams*, 21(11):112802, November 2018. Published 16 November 2018.
14. J. Zhu, Y. Chen, F. Brinker, W. Decking, S. Tomin, and H. Schlarb. High-fidelity prediction of megapixel longitudinal phase-space images of electron beams using encoder-decoder neural networks. *Phys. Rev. Appl.*, 16:024005, Aug 2021.
15. A. Sanchez-Gonzalez, P. Micaelli, C. Olivier, et al. Accurate prediction of x-ray pulse properties from a free-electron laser using machine learning. *Nat. Commun.*, 8:15461, 2017.
16. Olaf Ronneberger, Philipp Fischer, and Thomas Brox. U-net: Convolutional networks for biomedical image segmentation. In Nassir Navab, Joachim Hornegger, William M. Wells, and Alejandro F. Frangi, editors, *Medical Image Computing and Computer-Assisted Intervention – MICCAI 2015*, pages 234–241, Cham, 2015. Springer International Publishing.
17. Kaiming He, Xiangyu Zhang, Shaoqing Ren, and Jian Sun. Deep residual learning for image recognition. In *2016 IEEE Conference on Computer Vision and Pattern Recognition (CVPR)*, pages 770–778, 2016.
18. Ozan Oktay, Jo Schlemper, Loïc Le Folgoc, M. J. Lee, Matthias P. Heinrich, Kazunari Misawa, Kensaku Mori, Steven G. McDonagh, Nils Y. Hammerla, Bernhard Kainz, Ben Glocker, and Daniel Rueckert. Attention u-net: Learning where to look for the pancreas. *ArXiv*, abs/1804.03999, 2018.
19. Liang-Chieh Chen, George Papandreou, Florian Schroff, and Hartwig Adam. Rethinking atrous convolution for semantic image segmentation. *ArXiv*, abs/1706.05587, 2017.
20. Rosanne Liu, Joel Lehman, Piero Molino, Felipe Petroski Such, Eric Frank, Alex Sergeev, and Jason Yosinski. An intriguing failing of convolutional neural networks and the coorconv solution. In S. Bengio, H. Wallach, H. Larochelle, K. Grauman, N. Cesa-Bianchi, and R. Garnett, editors, *Advances in Neural Information Processing Systems*, volume 31. Curran Associates, Inc., 2018.
21. Matthew Tancik, Pratul Srinivasan, Ben Mildenhall, Sara Fridovich-Keil, Nithin Raghavan, Utkarsh Singhal, Ravi Ramamoorthi, Jonathan Barron, and Ren Ng. Fourier

features let networks learn high frequency functions in low dimensional domains. In H. Larochelle, M. Ranzato, R. Hadsell, M.F. Balcan, and H. Lin, editors, *Advances in Neural Information Processing Systems*, volume 33, pages 7537–7547. Curran Associates, Inc., 2020.

22. Yuxin Wu and Kaiming He. Group normalization. In Vittorio Ferrari, Martial Hebert, Cristian Sminchisescu, and Yair Weiss, editors, *Computer Vision – ECCV 2018*, pages 3–19, Cham, 2018. Springer International Publishing.